Convolution-Based Global Simulation Technique for Millimeter-Wave Photodetector and Photomixer Circuits

David B. Ameen and Gregory B. Tait, *Senior Member, IEEE*

***Abstract*—A fast convolution-based time-domain approach to global photonic-circuit simulation is presented that incorporates a physical device model in the complete detector or mixer circuit. The device used in the demonstration of this technique is a GaAs metal–semiconductor–metal (MSM) photodetector that offers a high response speed for the detection and generation of millimeter waves. Global simulation greatly increases the accuracy in evaluating the complete circuit performance because it accounts for the effects of the millimeter-wave embedding circuit. Device and circuit performance are assessed by calculating optical responsivity and bandwidth. Device-only simulations using GaAs MSMs are compared with global simulations that illustrate the strong interdependence between device and external circuit.**

***Index Terms*—Convolution, global simulation, millimeter-wave photodetector, photomixer.**

I. Introduction

MILLIMETER-WAVE detection and generation circuits using high-speed photodiodes are key components in today's optoelectronic-based communication and phased-array antenna systems [1]–[4]. Circuits that utilize a planar metal–semiconductor–metal (MSM) photodetector can provide the necessary bandwidth, responsivity, signal-to-noise ratio, and compatibility with monolithic optoelectronic integrated circuits [5]. Global simulation offers a time- and cost-effective means for optimizing the performance of complete MSM photodetector or photomixer circuits. It is necessary to include the embedding circuit in the simulation because the circuit presents an impedance to the active device that affects performance, with device parasitic capacitance and load resistance being major contributors to impedance. At high-frequency (HF) operation, both the device and circuit should be simulated in their full time-dependent mode of operation so that the full transient dynamics can be observed [6]. Dynamic device modeling is required to account for the response of carriers to HF signals. Although such simulations can be very computationally intensive, the present technique achieves accuracy with relatively low computational demand by using an efficient convolution-based time- domain approach to circuit simulation. Global simulation using a time-domain convolution approach is in contrast to more conventional harmonic-balance or optimization techniques [7], [8]. In order to simulate the dynamic operation of the device and its circuit, a physics-based carrier-transport formulation is used to model the nonlinear device, and an impulse response is used to characterize the linear embedding circuit.

The key features of the global simulator presented in this paper include advanced transport physics for the MSM Schottky contacts, accurate modeling of the embedding circuit's impulse response, and effective digital filtering of the impulse response for efficient convolution calculations. A description of the MSM physical-device model and the global simulation technique are given in Section II. Results from the simulation of individual MSM devices are compared with results of complete photodetector circuits in Section III, illustrating the effects of the external circuit on overall performance.

Manuscript received February 22, 2001; revised August 10, 2001.

D. B. Ameen is with the Department of Physics, Virginia Commonwealth University, Richmond, VA 23284 USA.

G. B. Tait is with the Electrical Engineering Department, Virginia Commonwealth University, Richmond, VA 23284 USA.

Digital Object Identifier 10.1109/TMTT.2002.803436.

II. Simulation

A. Device Model

The modeled device is a GaAs MSM photodetector with its electrodes in the trench formation, as shown in Fig. 1, which depicts a single MSM cell. This trench formation increases the optical response speed since the transit distance is short and the electric field is uniformly strong throughout the active region [9]. The dimensions of the device include depth $d = 1.0$ μm, substrate length $L_s = 1.1$ μm, half-contact length $L_c = 0.33$ μm, and contact width $W = 35.0$ μm. The GaAs has a donor background concentration of 3.5×10^{12} cm^{-3} so that the depletion region extends throughout the substrate, which maximizes the optical response speed. The net electric field is essentially one dimensional and establishes the single axis of carrier motion as the x-axis. The cross-sectional area for the photocurrent through the substrate is $A_{yz} = 35.0$ μm^2. The plane polarized light has wavelength $\lambda = 800$ nm, and enters the substrate along the y-axis. The cross-sectional area of the substrate surface exposed to the light is $A_{xz} = 38.5$ μm^2. The Schottky barrier height for both contacts is 1.0 eV.

Carrier transport in the device is modeled through the physics of the Boltzmann transport equation and Poisson's equation. Electron and hole currents are characterized by a drift–diffusion formulation, and the current continuity equations including optical generation and carrier recombination are solved self-consistently with Poisson's equation. These equations and the relevant GaAs material parameters are identical to those used in [10] and [11]. Boundary conditions are applied at the Schottky contacts. The nonlinear differential

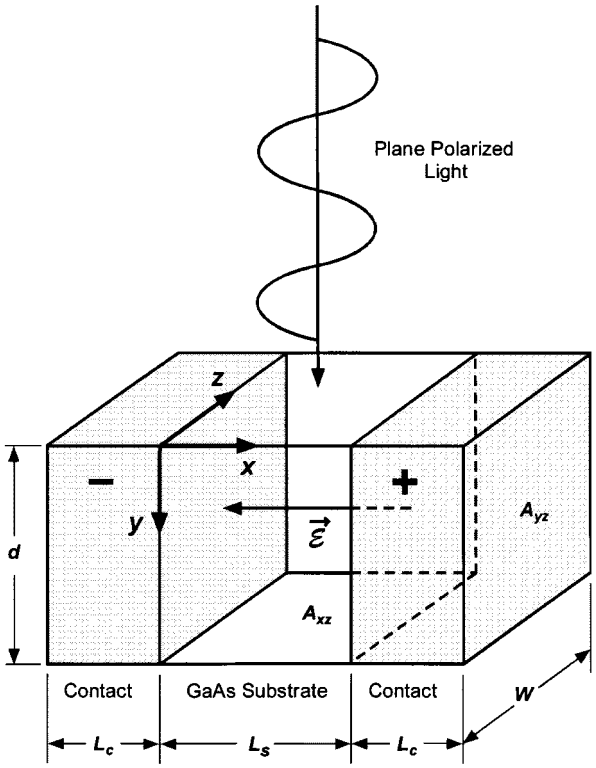

Fig. 1. Single MSM cell showing the substrate and contacts, a monochromatic lightwave, and the electric field $\boldsymbol{E}$ due to the applied voltage.

equations are discretized using finite differences and solved numerically using the Newton–Raphson iteration technique. Time stepping is accomplished using a full backward implicit scheme. Terminal current is computed at each time step, from which the current amplitude at the fundamental frequency is calculated so that the responsivity and bandwidth can be determined for a specific set of device and circuit parameters.

In this study, the current density boundary condition is an improved version of the combined drift–diffusion/thermionic emission (DD/TE) approach [10]. For the Schottky barrier at forward bias at $x = 0$, the current density $J_n(0)$ is given by

$$J_n(0) = q\left(F_n \upsilon_n n - \frac{1}{2}\upsilon_{n,0} n_0\right) \tag{1}$$

where q, n, n_0, F_n, and υ_n are the magnitude of the electron charge, electron density, electron density at equilibrium, fraction of electrons that move out of the semiconductor, and surface velocity of the electrons that move out of the semiconductor, respectively. The electron thermal velocity $\upsilon_{n,0}$ is given by

$$\upsilon_{n,0} = \sqrt{\frac{2k_B T}{\pi m_n^*}} \tag{2}$$

where k_B, T, and m_n^* are the Boltzmann's constant, Kelvin temperature, and electron effective mass, respectively. The surface velocity υ_n of the electrons that move out of the semiconductor is given by

$$\upsilon_n = \upsilon_{n,d} + \upsilon_{n,0}\frac{\exp(-\lambda_n^2)}{1+\operatorname{erf}(\lambda_n)} \tag{3}$$

in which λ_n is given by

$$\lambda_n = \frac{1}{\sqrt{\pi}}\frac{\upsilon_{n,d}}{\upsilon_{n,0}} \tag{4}$$

and the effective electron drift–diffusion velocity $\upsilon_{n,d}$ is given by

$$\upsilon_{n,d} = \frac{J_n}{qn}. \tag{5}$$

Parameters are evaluated at a point in the semiconductor just inside of the contact. In this advanced boundary condition, the fraction of electrons F_n that move out of the semiconductor is also considered, and is given by

$$F_n = \frac{1}{2}\left[1+\operatorname{erf}(\lambda_n)\right]. \tag{6}$$

The electron current density at $x = L_s$, as well as the hole current density at both boundaries, are given by equations similar to (1).

The electron and hole current continuity equations contain a net carrier recombination term and an optical carrier generation term. The recombination rate R is characterized by a Shockley–Read–Hall model [12] given by

$$R = \frac{np - n_i^2}{\tau_n(p+p_t)+\tau_p(n+n_t)} \tag{7}$$

where n_i is the intrinsic carrier density, p is the hole density, τ_n and τ_p are the electron and hole lifetimes, respectively (which, in this study, are set equal to each other or $\tau_n = \tau_p = \tau$), and n_t and p_t are the electron and hole trap constants, respectively. The optical generation rate G_L is given by [13]

$$G_L = \frac{\xi_0}{h\nu d}\frac{L_s}{L_s+2L_c}(1-r)\left[1-\exp(-\alpha d)\right]\left[1+M\sin(\omega t)\right] \tag{8}$$

where ξ_0 is the incident light intensity, h is Planck's constant, ν is the frequency of the 800-nm light, the reflectance $r = 0.32$, the light absorption coefficient $\alpha = 1.7\times 10^4$ cm^{-1}, the modulation index $M = 0.9$, and ω is the optical carrier modulation frequency or difference frequency from the optical heterodyning of two carrier lasers. With these parameter values, the external quantum efficiency is 16%.

Carrier mobility can be modeled by either the field-independent or field-dependent approaches [12]. The field-dependent mobility model is recommended for the high electric fields encountered in MSM photodetectors, provided the device length is sufficient for carrier energy to reach a steady state with the local electric field and lattice scattering. However, at very high modulation frequencies, the carrier energy may not reach such a steady state with the local field, and this nonsteady-state transport might be more closely modeled by field-independent mobility. The low-field values of mobility for electrons and holes are 7200 cm^2/V-s and 380 cm^2/V-s, respectively, in the GaAs material.

The accuracy of the device simulator was calibrated by comparing simulation results for dc current–voltage characteristics of Schottky and MSM devices with experimental data in the literature [14]. Further calibrations were conducted by comparing

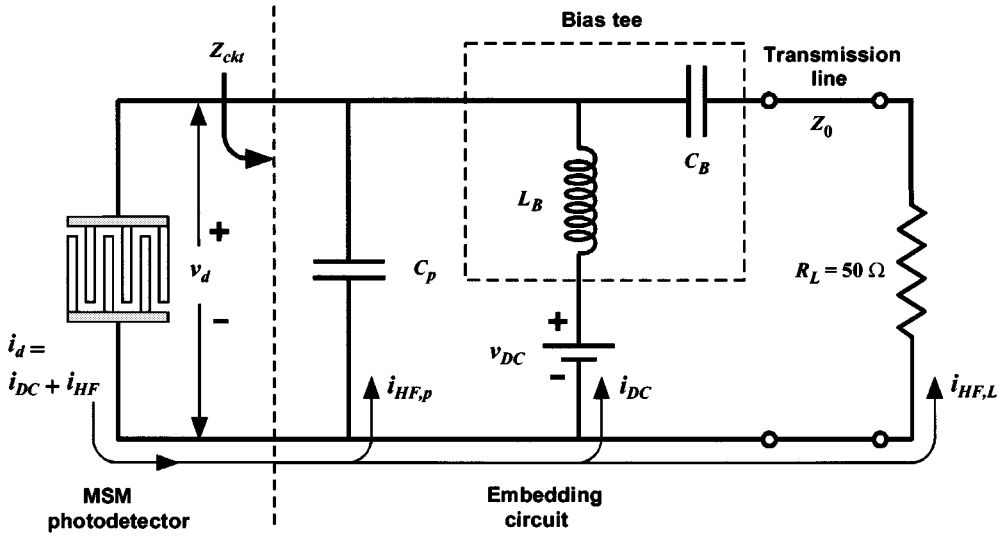

Fig. 2. Photodetector circuit with MSM device.

simulated versus measured optical responsivities of an MSM device illuminated by an unmodulated light carrier. Comparisons using the field-dependent mobility model were excellent in these test cases. Therefore, we use the drift–diffusion model with field-dependent mobility for carrier transport in this paper. These models should remain valid for optical signals modulated up to 100 GHz, and mark an improvement over quasi-static models.

B. Global Model

The global model for the photodetector circuit consists of the device integrated into its linear embedding circuit, as shown in Fig. 2. A bias tee is used to separate the HF and dc signals so that only the HF signals generated by the photodetector are delivered to the load resistance R_L. The load resistance is taken to be matched to the transmission-line impedance Z_0 at the millimeter-wave output. A small portion of the HF signal $i_{\mathrm{HF},p}$ is carried by the branch with the parasitic capacitance C_p, while the main current component $i_{\mathrm{HF},L}$ is carried by the branch with the load resistance. The parasitic capacitance C_p models inter-electrode and other stray capacitance effects external to the device active region. It does not include the intrinsic device capacitance that is part of the varying electric field and dynamic carrier transport calculated by the numerical device simulator. As the frequency is increased, more signal is shunted through the parasitic capacitance. The output from the circuit is that portion of the signal that is carried in the load resistance and is the primary quantity sought through the global simulation.

The linear embedding circuit creates an impedance Z_{ckt} presented to the terminals of the device. The impulse response function z_{ckt} is calculated once by performing an inverse fast Fourier transform (IFFT) on the embedding impedance function Z_{ckt}

$$Z_{ckt}(j\omega) \Rightarrow \mathrm{IFFT} \Rightarrow z_{ckt}(t). \tag{9}$$

The relationship between device terminal current $i_d(t)$ and voltage $v_d(t)$ as a function of time can be determined by performing a convolution that includes the impulse response function z_{ckt}

$$v_d(t) = v_{\mathrm{DC}} - \int_0^t z_{ckt}(t-\tau) i_d(\tau)\, d\tau. \tag{10}$$

In general, due to the distributed reactive nature of microwave circuits, the embedding impedance can be determined in the frequency domain directly from microwave measurements or electromagnetic-field simulators that solve Maxwell's equations in three dimensions, such as HFSS.[1] This process only needs to be performed once for a given embedding circuit. A simpler approach for determining the embedding impedances is used in the present study by making an equivalent circuit model of the actual circuit (Fig. 2). The equivalent embedding circuit impedance $Z_{ckt}(j\omega)$ is

$$Z_{ckt}(j\omega) = \left(j\omega C_p + \frac{1}{j\omega L_B} + \frac{1}{\dfrac{1}{j\omega C_B} + R_L} \right)^{-1} \tag{11}$$

where $j\omega$ is the complex angular frequency. Typical values for the passive elements are used to generate the impedance function. These include load resistance $R_L = 50\ \Omega$, bias-tee capacitance $C_B = 5$ pF, bias-tee inductance $L_B = 5$ nH, and parasitic capacitance $C_p = 100$ fF. The final impedance function is discretized, with the impedance samples given by

$$Z_m = Z_{ckt}(m\Delta f), \qquad m = 0 \cdots M \tag{12}$$

where the frequency $f = \omega/(2\pi)$, and the impedance values are calculated up to the Nyquist frequency ($M\Delta f$) with the Nyquist frequency being one-half of the reciprocal of the time step used in the device simulator.

By taking the IFFT of the impedance samples, the discrete-time impulse response for the embedding circuit is

[1]High-Frequency Structure Simulator (HFSS), rel. 5.6, Hewlett-Packard Company, Santa Rosa, CA, 2000.

generated. Since the frequency step Δf must be small enough to avoid aliasing effects in the impulse response, a large number of impedance samples are required. Therefore, the corresponding number $2M + 1$ of discrete-time impulse response samples is large, on the order of 10^4–10^5. In order to achieve a faster global simulation, the impulse response sequence could be truncated, which could limit the accuracy of the simulation. However, an asymmetric Kaiser filter [6] can be used to reshape and taper the impulse response to preserve accuracy, with the filter function given by

$$w_n = \begin{cases} c, & 0 \le n \le N_1 \\ \dfrac{c \cdot I_0\left[\beta\sqrt{1-\left(\dfrac{n-N_1}{N_2-N_1}\right)^2}\right]}{I_0(\beta)}, & N_1 < n \le N_2 \\ 0, & n > N_2 \end{cases} \tag{13}$$

where c, β, and N_1 are shaping factors, N_2 is the truncation index for the sequence, I_0 is the modified Bessel function, and w_n is the filter weight for the nth impulse response sample. The filtered sample h_n is calculated by multiplying the unfiltered impulse response sample $z_{ckt,n}$ by its filter weight w_n. The advantage gained by filtering is that N_2 is on the order of 10^3–10^4, which is up to two orders of magnitude smaller than the original impulse response sequence. To show that the filtered impulse response samples preserve the original embedding impedance function, it is necessary to transform the filtered impulse response back to the frequency domain and compare the reconstructed impedance function with the original. The shaping factors in (13) are adjusted to give the best possible reproduction of the original embedding impedance.

The discrete convolution used in the global simulator is given by

$$v_k = v_{\mathrm{DC}} - \sum_{j=k-N_2+1}^{k-1} h_{k-j} i_j(v_j) + h_0 i_k(v_k) \tag{14}$$

where k represents the time-step level ($k\Delta t$) and v and i are the terminal voltages and currents of the device. Equation (14) is in fixed-point iteration form, and the kth current sample is separated from the other terms because i_k is the only unknown current sample. To speed the iterative process, the unknown i_k can be approximated by the linear extrapolation $i_k \approx 2i_{k-1} - i_k$, provided the time step Δt is sufficiently small. The global circuit algorithm steps are as follows:

Step 1) predict the device current i_k for the present time step based on the known previous currents;
Step 2) use the discrete convolution to generate the device voltage v_k for the present time step;
Step 3) use the device simulator with the device voltage v_k from step 2) to calculate the corrected current i_k;
Step 4) check the percent difference between the prediction and correction for i_k;
Step 5) iterate if necessary.

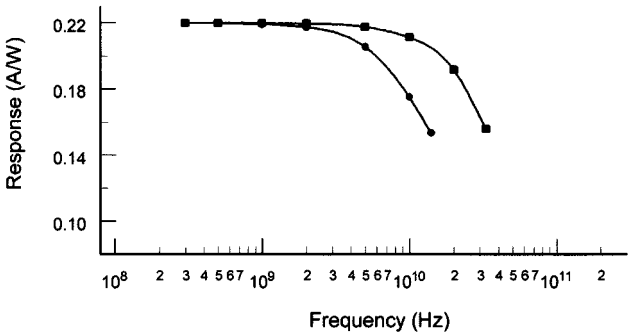

Fig. 3. Comparison of frequency response for 1- (—●—) and 10-V (—■—) dc-bias voltages.

Experience to date has shown that step 5) is usually not necessary for the small time steps Δt typically used in device simulations, which greatly speeds the global simulation.

III. Results

A. Device-Only Simulations

Simulations are first run with the device alone, under conditions of an applied constant dc voltage bias and a modulated light carrier incident on the device. The conventional-growth-temperature (600 °C) GaAs material used in this study is characterized by a long carrier lifetime $\tau = 10^{-8}$ s [15], [16]. The results are presented in Fig. 3 through a comparison of frequency response curves for two values of applied bias voltage (1 and 10 V). The incident light intensity is 1 kW/cm^2. The low-frequency responsivity is approximately 0.22 A/W for both bias voltages.

Bandwidth for the device simulations are dependent on transit time and the effective carrier lifetime, with the shorter time being the major factor in determining bandwidth. Transit time is affected by the mobility model, applied bias voltage, and screening of the electric field by excess photogenerated charge carriers. At 1-V dc bias in Fig. 3, the average transit times for electrons and holes are approximately 4 and 17 ps, respectively. At 10-V dc bias, the electron velocity decreases to its saturation velocity, causing the average electron transit time to increase slightly to 6 ps. The hole velocity at 10-V bias, however, increases significantly, and the average hole transit time decreases to 9 ps. For this long-carrier-lifetime GaAs material, the bandwidth is primarily determined by these transit times. The 3-dB bandwidths are 14 and 33 GHz for 1- and 10-V bias cases, respectively.

B. Global Simulations

The presence of the embedding circuit is expected to alter the performance relative to the device-only simulation. The bandwidth should be affected because the reactance in the embedding circuit slows the response of the overall circuit. In order to determine the effect of the embedding circuit, the photocurrents delivered to the load that result from the global simulations are compared to the short-circuit currents from the device-only simulations.

Global bandwidth is determined by the interaction between the device response time τ_d and the circuit response time τ_{RCp}.

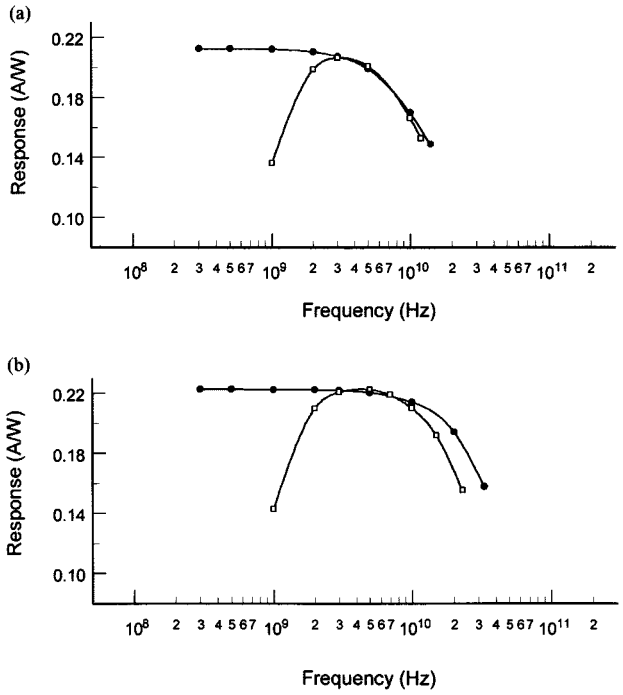

Fig. 4. Comparison of frequency response for device-only (—●—) and global (—□—) simulations at: (a) 1- and (b) 10-V dc bias voltages.

TABLE I
RESPONSIVITY AND BANDWIDTH FOR DEVICE-ONLY AND GLOBAL SIMULATIONS

DC Bias Voltage	Device-Only			Global	
	R_{opt} (A/W)	f_{3-dB} (GHz)	τ_d (ps)	R_{opt} (A/W)	f_{3-dB} (GHz)
1 V	0.21	14	11.4	0.21	12
10 V	0.22	33	4.8	0.22	23

The device response time τ_d is defined from the bandwidth $f_{3\text{-dB}}$ of the device-only response (given in Section III-A) as

$$\tau_d = \frac{1}{2\pi f_{3\text{-dB}}}. \tag{15}$$

The response time τ_{RCp} of the simple embedding circuit is defined as

$$\tau_{RCp} = R_L C_p. \tag{16}$$

Based on (16), the circuit time constant used in this study is $\tau_{RCp} = 5$ ps, for $R_L = 50\ \Omega$ and parasitic capacitance of $C_p = 100$ fF. The corresponding cutoff frequency given by

$$f = \frac{1}{2\pi\tau_{RCp}} \tag{17}$$

is $f = 32$ GHz.

Simulation results are presented in Fig. 4 through a comparison of responsivity versus frequency for the same two dc-bias voltages (1 and 10 V), and incident light intensity (1 kW/cm^2) that were used previously for the device-only simulations. Table I lists the optical responsivities R_{opt} and bandwidths $f_{3\text{-dB}}$.

In the low-bias voltage case, shown in Fig. 4(a), the HF cutoff for the two simulations is consistent with the device response time $\tau_d = 11.4$ ps being longer than $\tau_{RCp} = 5$ ps. Hence, the device response time τ_d limits the global simulation bandwidth. In the high-bias voltage case, shown in Fig. 4(b), the global response is quite different from the device-only response. This result is consistent with the device response time $\tau_d = 4.8$ ps being comparable to τ_{RCp}. Therefore, the global bandwidth depends strongly on the interaction between device and circuit, yielding a reduced 3-dB frequency cutoff of 23 GHz. The low-frequency cutoff in the global simulation is entirely due to the effect of the bias-tee circuitry.

IV. CONCLUSION

The global simulation used in the present study calculates the relationship between terminal voltage and current as functions of time for a GaAs MSM photodetector with trench electrodes. Both the physics-based device and the embedding circuit impulse response are modeled in the time domain. A new convolution-based algorithm is used to characterize the photodetector circuit, and enables a fast global simulation. Two key features are the reshaping of the impulse response through digital filtering, which reduces the number of discrete time samples by up to two orders of magnitude, and the use of a linear predictor for the current so that the number of fixed-point iterations in the convolution algorithm can be reduced to one. This convolution technique was demonstrated in a simple photodetector circuit using the drift–diffusion model for the MSM device. This same technique can be employed directly with more complex circuits and more complete physical device models, such as energy balance or Monte Carlo approaches, to give a complete global simulation of photonic circuits above 100 GHz.

REFERENCES

[1] S. Pajarola, G. Guekos, P. Nizzola, and H. Kawaguchi, "Dual-polarization external-cavity diode laser transmitter for fiber-optic antenna remote feeding," *IEEE Trans. Microwave Theory Tech.*, vol. 47, pp. 1234–1240, July 1999.

[2] U. Gliese, T. N. Nielson, S. Norskov, and K. E. Stubkjaer, "Multifunctional fiber-optic microwave links based on remote heterodyne detection," *IEEE Trans. Microwave Theory Tech.*, vol. 46, pp. 458–468, May 1998.

[3] R. P. Braun, G. Grosskopf, H. Heidrich, C. von Helmolt, R. Kaiser, K. Kruger, U. Kruger, D. Rohde, F. Schmidt, R. Stenzel, and D. Trommer, "Optical microwave generation and transmission experiments in the 12- and 60-GHz region for wireless communications," *IEEE Trans. Microwave Theory Tech.*, vol. 46, pp. 320–329, Apr. 1998.

[4] M. Y. Frankel, P. J. Matthews, and R. D. Esman, "Fiber-optic true time steering of an ultrawide-band receive array," *IEEE Trans. Microwave Theory Tech.*, vol. 45, no. 8, pp. 1522–1526, Aug. 1997.

[5] G. B. Tait, A. H. Sayles, B. C. Tousley, A. Paolella, and P. Cooke, "High-performance GaAs metal–semiconductor–metal photodetectors grown at intermediate temperatures," in *Photodetectors: Materials and Devices*, G. J. Brown and M. Razeghi, Eds. Bellingham, WA: SPIE, 1996, Proc. SPIE 2685, pp. 163–170.

[6] G. B. Tait and S. H. Jones, "Transient simulation of millimeter-wave circuits incorporating numerical device modeling," *IEEE Trans. Microwave Theory Tech.*, vol. 47, pp. 877–881, June 1999.

[7] G. B. Tait, "Efficient solution method for unified nonlinear microwave circuit and numerical solid-state device simulation," *IEEE Microwave Guided Lett.*, vol. 4, pp. 420–422, Dec. 1994.

[8] J. Grajal, V. Krozer, E. Gonzalez, F. Maldonado, and J. Gismero, "Modeling and design aspects of millimeter-wave and submillimeter-wave Schottky diode varactor frequency multipliers," *IEEE Trans. Microwave Theory Tech.*, vol. 48, pp. 700–711, Apr. 2000.

[9] L. Laih, T. Chang, Y. Chen, W. Tsay, and J. Hong, "Characteristics of MSM photodetectors with trench electrodes on p-type Si wafer," *IEEE Trans. Electron Devices*, vol. 45, pp. 2018–2023, Sept. 1998.
[10] J. R. Jones, G. B. Tait, S. H. Jones, and D. S. Katzer, "DC and large-signal time-dependent electron transport in heterostructure devices: An investigation of the heterostructure barrier varactor," *IEEE Trans. Electron Devices*, vol. 42, pp. 1393–1403, Aug. 1995.
[11] M. S. Lundstrom and R. J. Schuelke, "Numerical analysis of heterostructure semiconductor devices," *IEEE Trans. Electron Devices*, vol. ED-30, pp. 1151–1159, Sept. 1983.
[12] S. Selberherr, *Analysis and Simulation of Semiconductor Devices*. Wien, NY: Springer-Verlag, 1984.
[13] I. S. Ashour, J. Harari, J. Vilcot, and D. Decoster, "High optical power nonlinear dynamic response of AlInAs/GaInAs MSM photodiode," *IEEE Trans. Electron Devices*, vol. 42, pp. 828–834, May 1995.
[14] D. B. Ameen, "Global simulation of a GaAs metal–semiconductor–metal photodetector for the conversion of optical signals into microwaves," Ph.D. dissertation, Dept. Phys., Virginia Commonwealth Univ., Richmond, VA, 2000.
[15] S. Gupta, M. Y. Frankel, J. A. Valdmanis, J. F. Whitaker, G. A. Mourou, F. W. Smith, and A. R. Calawa, "Subpicosecond carrier lifetime in GaAs grown by molecular beam epitaxy at low temperature," *Appl. Phys. Lett.*, vol. 59, no. 25, pp. 3276–3278, Dec. 1991.
[16] B. Nabet, A. Paolella, P. Cooke, M. Lemuene, R. Moerkirk, and L.-C. Liou, "Intermediate temperature molecular beam-epitaxy growth for design of large-area metal–semiconductor–metal photodetectors," *Appl. Phys. Lett.*, vol. 64, no. 23, pp. 3151–3153, June 1994.

David B. Ameen received the B.S. degree in biology education and M.S. degree in biophysics from the University of Virginia, Charlottesville, in 1976 and 1987, respectively, and the M.S. degree in physics and Ph.D. degree in chemical physics from Virginia Commonwealth University (VCU), Richmond, in 1996 and 2000, respectively.

He is currently a faculty member in the Department of Physics, Virginia Commonwealth University. He previously taught science and mathematics at the secondary level for 11 years. His areas of research interests include physical device modeling and global simulation of photonic circuits and properties of lightwave propagation through collagen fibers in the cornea of the eye.

Gregory B. Tait (S'83–A'83–M'84–SM'95) received the B.A. degree in physics from Amherst College, Amherst, MA, in 1982, the M.S. degree in electrical engineering from the University of Maryland at College Park, in 1984, and the Ph.D. degree in electrical engineering from the Johns Hopkins University, Baltimore, MD, in 1991.

He is currently an Associate Professor of electrical engineering with Virginia Commonwealth University (VCU), Richmond. Prior to joining the School of Engineering, VCU, in 1996, he was a member of the electrical engineering faculty with the U.S. Military Academy, West Point, NY. His other professional experience includes 12 years of research and design engineering in semiconductor devices with the Naval Research Laboratory, Washington, DC, and satellite communications with Fairchild Industries, Germantown, MD. His areas of research interests include development of novel semiconductor devices for microwave and photonic circuits, numerical modeling and computer simulation of physical electronic transport in solid-state materials, and applied electromagnetics.

Dr. Tait is a member of the IEEE Microwave Theory and Techniques Society (IEEE MTT-S), and serves on the IEEE MTT-1 Technical Committee on computer-aided design.